

Baseline Removal in Spectrometry Gamma by Observation of Local Minima

Kélian This

Commissariat à l'énergie atomique (CEA)
Nuclear measurement laboratory
 21120, Valduc, France
 kelian.this@cea.fr

Laurent Le Brusquet

Université Paris-Saclay, CNRS, CentraleSupélec
Laboratoire des signaux et systèmes
 91190, Gif-sur-Yvette, France

Adrien Frigerio

Commissariat à l'énergie atomique (CEA)
Nuclear measurement laboratory
 21120, Valduc, France

Sébastien Colas

Commissariat à l'énergie atomique (CEA)
Nuclear measurement laboratory
 21120, Valduc, France

Pascal Bondon

Université Paris-Saclay, CNRS, CentraleSupélec
Laboratoire des signaux et systèmes
 91190, Gif-sur-Yvette, France

Abstract—This paper presents a Baseline Removal method in the context of spectrometry gamma. The method implements an estimator for the full continuum based on the observation of local minima. This estimator is constructed from the statistical properties of the signal and is therefore easily explainable. The method involves a limited number of fixed parameters, which allows the automation of the process. Moreover, the method is adaptable to any peaks width, which makes it suitable for both HPGe spectrometers and scintillators. Application to real gamma spectrometry measurements are presented, as well as a discussion about the choice of the parameters, for which an adjustment is proposed.

Index Terms—background removal, baseline correction, gamma spectrometry, continuum estimation, peak characterization, local minima

I. INTRODUCTION

A. Context

Gamma spectrometry is a common nuclear measurement technique which can be used for the detection of radioactivity, identification of radionuclides, and quantification of radioactive material. Eventhough other methods exist, in practice, the gamma spectrometry often constitutes the only possible and effective technique, especially for waste characterization [1]. As a consequence, gamma spectrometry has become essential in the nuclear sector.

One will find in [2] a complete description of gamma rays Physics as well as a number of details relating to the measurement device. The result of a measurement is a histogram, called spectrum, which spreads detected photons by channels each corresponding to an interval of energy. All spectra have the same structure, that is to say a superposition of a background with peaks specific

to some radionuclides, covered by an observation noise. Peaks are mathematically described by a mixture model, usually Gaussian [2, section 9.6] [3, p.229] but not only [4], which contains a great deal of useful information. On the opposite, the background, also called continuum which is rather regular and smooth contains few information (at least, with regard to the peaks).

The purpose of the spectrum analysis is to estimate the mixture parameters from the data. Consequently, continuum is of little interest and one of the major issue of the spectrum analysis is to isolate the mixture from the continuum. Baseline Removal (BR) methods enable to estimate the continuum without any consideration for the peak mixture, then to subtract it from the spectra in order to isolate the peak mixture. This technique can also be found in Literature under the appellation "background correction", or a mix of both expressions. However, "baseline" is less ambiguous than "background" which may also refers to the radiation from the environment. Moreover, "removal" is more appropriate that "correction" because it would implies the continuum to be an error, which is not the case.

B. State of the Art

BR techniques is is a recurrent topic in gamma spectrometry, but also in other spectroscopy issues [5]. From the very beginning in the 70s to nowadays, two distinct strategies have been brought to light: local and global.

Local Baseline Removal (LBR) methods enable to estimate derive a local estimate of the continuum on a given Region Of Interest (ROI) of the spectrum, i.e. in the vicinity of a peak, by the observation of points of the pure continuum at the outer left and right borders of the ROI

[6] [7] [8] [9] [2, sections 5.4]. LBR requires to established the ROI beforehand by the use of a Peak Detection (PD) method.

Full Baseline Removal (FBR) methods estimate the whole continuum of the spectrum, without introducing the concept of ROI, and does not rely on a PD method. Among FBR techniques, one finds filtering [10], peak erosion [11] [12] [13] [3, p.256] [14], penalizing or regularization criterion [15] [16] [17] [18] [19] [20] [21] [22] [23], and observation of local minima [24] [25] [26] [27] [28] [29].

Nowadays, those propositions were naturally ranked by the operating experience, and LBR [2, sections 5.4] coupled to the PD second derivative method [30] is commonly used and officially recommended [31] [32]. This method chiefly draws its success from its simplicity and explainability. However, it remains difficult to be automated and may fail in the presence of Compton edges or multiplets, i.e. mixtures of close overlapping peaks. On the other hand, a large number of proposed global methods involve a model for the continuum (splines, Gaussian processes etc), which introduce an improper regularity prior: continuum often contains discontinuities which are difficult to model. Thus, spectrum analysis is still an active research topic.

C. Content

Beyond the performance criterion, an ideal method should enables the automation of the analysis with a large scope of application. It shall deal with various peaks shapes and widths, with various radiation detectors technologies, i.e. Hyper Pure Germanium (HPGe) detectors as well as scintillators. The method shall admit a reduced set of parameters independent from the observation.

The central idea of the present study relies on the following empirical observation: local minima rarely appear on peaks. Thus, it would be possible to estimate the continuum from local minima. As mentioned in the state of the Art, several authors have approached this idea, but the work of Tervo et al. [27] is the most accomplished: it enables to simplify the estimation of the continuum without any prior nor any parameters. However, this estimator only works with thin peaks which quickly limits its use for real applications.

This paper takes up, corrects and extends previous developments [33]. This work presents a BR method adapted to gamma spectrometry also based on the observation of local minima. Fig. 1 presents the application of the method of Tervo and of the new method on two representative spectra. The improvement is easily noticeable on the figure, and shows that the new method covers a much wider range of spectra configurations (the comparison will be detailed in part IV). The resulting process is simple to apply. The paper is focused on the statistical phenomenon which enables the method to give good results.

Section II, on one hand, gives a definition of the spectrum. On the other hand, it deducts a number of inherent signal properties on which is built the continuum

estimation procedure in section III. Section IV comments the real spectra application, and section V concludes this work.

II. SPECTRUM SIGNAL PROPERTIES

This section aims at formalizing the problem and proposes some general properties about a gamma spectrum and its components.

A. Basic assumptions

Let \mathbf{y} denote the observed gamma spectrum of n channels such that $\mathbf{y} = (y_1, \dots, y_n)$. Let $\mathbf{m} = (m_1, \dots, m_n)$ denote the peaks mixture and $\mathbf{c} = (c_1, \dots, c_n)$ the continuum. Denoting \mathcal{P} the Poisson's distribution, Physics states [2, section 5.2] \mathbf{y} is a sample from a random vector $\mathbf{Y} = (Y_1, \dots, Y_n)$ such that:

$$Y_k \sim \mathcal{P}(\mu_k) \quad (1)$$

where $\boldsymbol{\mu} = \mathbf{m} + \mathbf{c}$ is the noiseless signal.

Poisson distribution is not practical to handle in literal calculations. Denoting \mathcal{N} the normal distribution and assuming that the spectrum has a sufficient number of count per channel, the following approximation is possible [34, section 2.7.3]:

$$\mathcal{P}(\mu_k) \approx \mathcal{N}(\mu_k, \mu_k) \quad (2)$$

By the properties of the Poisson distribution [34, section 13.5.5], y_k is itself an estimate for μ_k and the associated confidence interval with symmetric risks of level $1 - \eta$ is:

$$\frac{1}{2}\chi_{2y_k; \eta/2}^2 \leq \mu_k \leq \frac{1}{2}\chi_{2(y_k+1); 1-\eta/2}^2 \quad (3)$$

where $\chi_{v; \eta}^2$ is the quantile of order η of a χ^2 distribution with v degrees of freedom. Using this property in order to quantify the variance of the observation, one may assume the following hypothesis:

Hypothesis 1:

$$\begin{cases} Y_k \sim \mathcal{N}(\mu_k, \sigma_k^2) \\ \sigma_k^2 = y_k \end{cases} \quad (4)$$

The issue can now be specified: knowing \mathbf{y} , how to estimate \mathbf{c} ? Because \mathbf{m} is also unknown, the problem is unsolvable at this stage: a prior is required. In the paragraphs below, one is looking for a discrimination criterion, through the definitions of peaks and continuum, which may be used as the missing constraint.

B. Signal characterization

Let introduce the differential operator $\Delta x_k = x_k - x_{k-1}$. The continuum is characterized by its low variations. Thus, continuum variations are majorated:

$$\exists \beta, \forall k, |\Delta c_k| \leq \beta \quad (5)$$

A peak has characteristic areas. A top, at the center, has high values and low variations. Two flanks, uprising and downrising on both sides of the top, have high variations, especially in comparison with continuum variations. Two

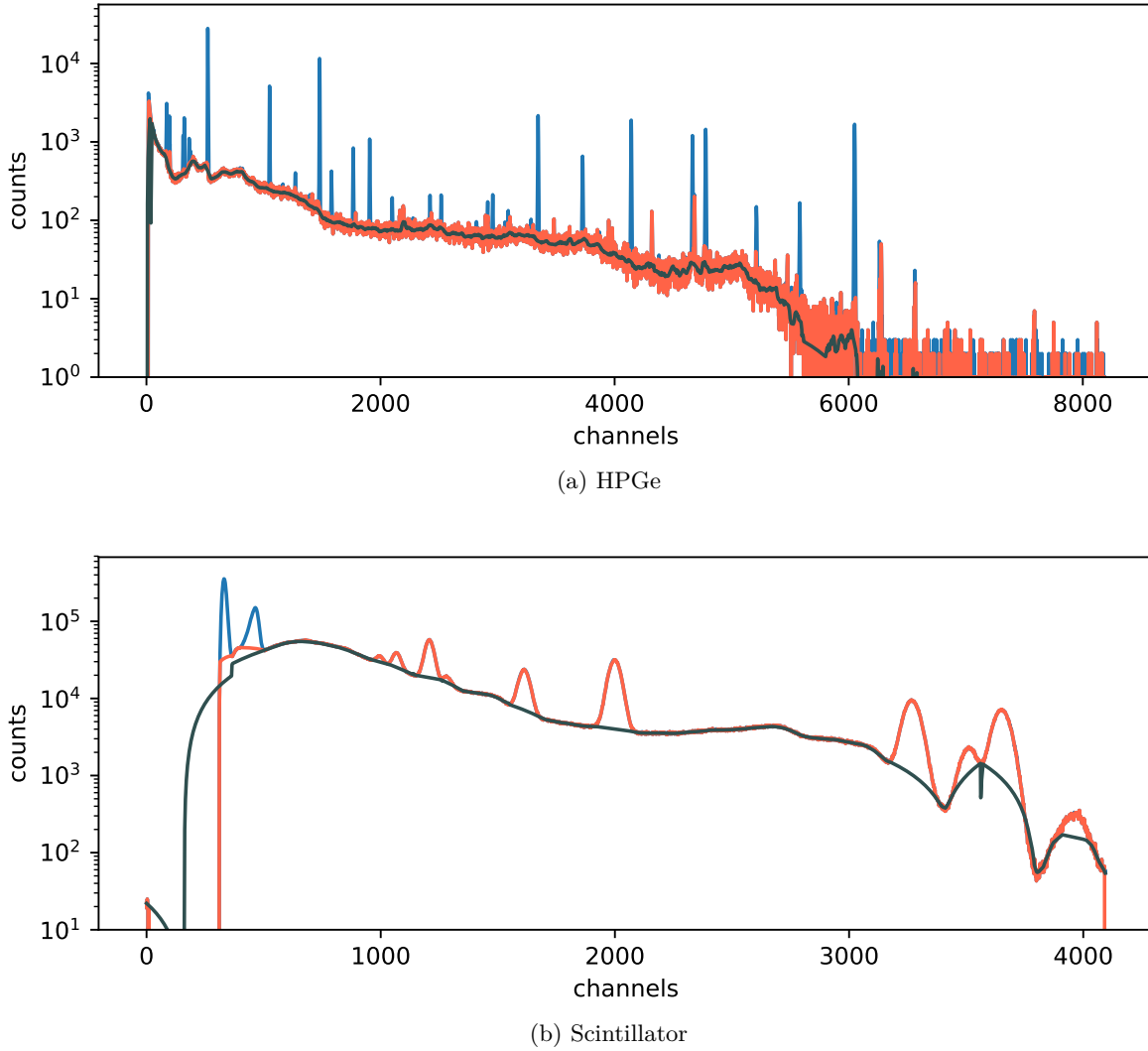


Fig. 1: Confrontation of continuum estimation methods on real spectra. On top is a HPGe spectrum, on the bottom a scintillator spectrum. Both are plotted with a log scale. Blue lines represent the observation. Orange lines represent the reference estimates of Tervo's method. Black lines represent the new method results, applied with parameters $t_{\text{break}} = 3$, $w_{\text{opt}} = 15$, $w_f = 11$, $o_f = 1$ and $w = 6$ for HPGe, $w = 80$ for scintillator.

flats at the borders have low values and low variations. Let denote \mathbb{F} the set of all flanks in the spectrum. Then, $\overline{\mathbb{F}}$ contains all tops and flats. The borders of the areas are thereby defined by means of a threshold α such that:

$$\beta \leq \alpha, \quad \forall k \in \mathbb{F}, \quad \alpha \leq |\Delta m_k| \quad (6)$$

The unfixed threshold α is a necessary scaling variable, and its choice is a matter of convention. Indeed, what could be considered as a peak in a certain context could be considered as a continuum contribution in another. Fig. 2 shows a mono peak signal with a constant continuum. Choosing $\alpha = 50$, resulting \mathbb{F} areas are represented with grey bands.

As a consequence of the previous definitions, one can deduce a lower bound for the variations of the signal:

Property 1:

$$\forall k \in \mathbb{F}, \quad \alpha - \beta \leq |\Delta \mu_k| \quad (7)$$

C. Counter variations

Let denote respectively \mathbb{F}^+ and \mathbb{F}^- the set of increasing flanks and the set of decreasing flanks:

$$\begin{cases} \mathbb{F}^+ &= \{k \in \mathbb{F} | \alpha \leq \Delta m_k\} \\ \mathbb{F}^- &= \{k \in \mathbb{F} | \Delta m_k \leq -\alpha\} \end{cases} \quad (8)$$

$\forall k \in \mathbb{F}$ let F_k be the probability to have a counter-variation in \mathbf{y} at k . More specifically, F_k is the probability

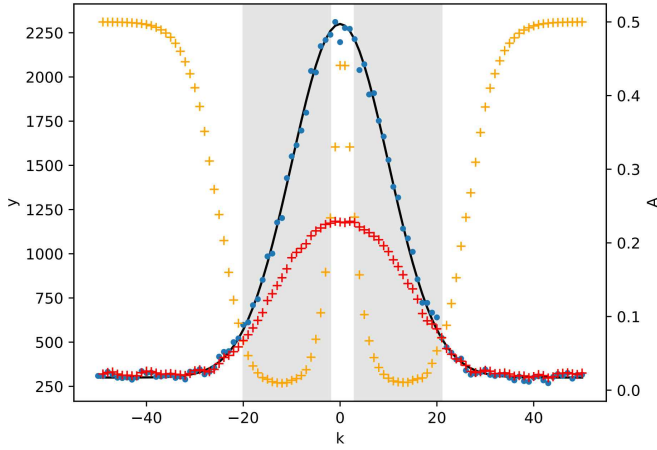


Fig. 2: Identification of peak's areas on a Gaussian example. Dark full line represents the signal μ , blue points represent observations \mathbf{y} , grey bands indicates \mathbb{F} , orange crosses represent \mathbf{A}^{lim} , red crosses represent \mathbf{A} .

for \mathbf{y} to decrease where \mathbf{m} is increasing, or to increase where \mathbf{m} is decreasing:

$$F_k = P(\Delta Y_k \leq 0 | k \in \mathbb{F}^+) \quad (9)$$

$$= P(0 \leq \Delta Y_k | k \in \mathbb{F}^-) \quad (10)$$

Notice that F_k is almost the repartition function of $\Delta Y_k \sim \mathcal{N}(\Delta \mu_k, \sigma_k^2 + \sigma_{k-1}^2)$ evaluated at 0. Let denote $\Phi(\cdot)$ the cumulative distribution function (CDF) of the standard normal distribution. Thanks to property 1 and noticing Φ is an increasing function, one has an upper bound for F_k :

Property 2:

$$\forall k \in \mathbb{F}, \quad F_k \leq A_k = \Phi\left(\frac{-(\alpha - \beta)}{\sqrt{\sigma_k^2 + \sigma_{k-1}^2}}\right) \quad (11)$$

On Fig. 2 is plotted $\mathbf{A} = (A_1, \dots, A_n)$ for $\alpha = 50$ and $\beta = 0$. Because this signal is a simulation, one exactly knows the value of Δm_k , which allows to evaluate the admissible limit values for \mathbf{A} as follows:

$$A_k^{lim} = \Phi\left(\frac{-\Delta m_k}{\sqrt{\sigma_k^2 + \sigma_{k-1}^2}}\right) \quad (12)$$

One notes through $\mathbf{A}^{lim} = (A_1^{lim}, \dots, A_n^{lim})$ that counter-variations probabilities are close to zero on high variations areas. This observation is confirmed by Fig. 3 where the value of A_k quickly decreases.

D. Focus on local minima

Let introduce ξ , the set of indexes of \mathbf{y} local minima:

$$\xi = \{k | y_k < y_{k-1}, y_k < y_{k+1}\} \quad (13)$$

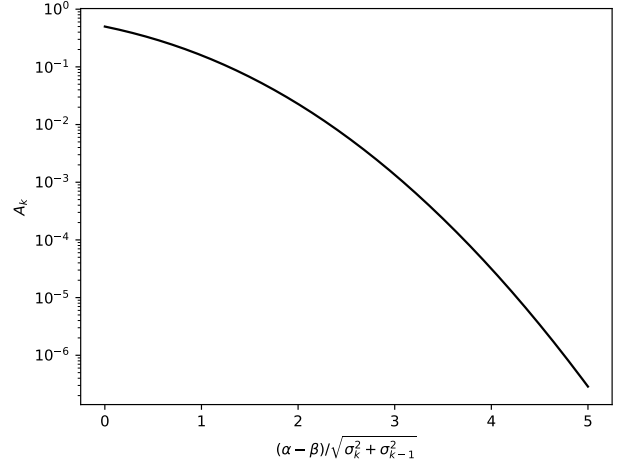


Fig. 3: A_k values on a log scale.

1) *Local minima bias:* As shown in Fig. 4, the local minima set is biased because local minima's expectation is not equal to the signal expectation. Moreover, the figure shows that local minima are less dispersed than the observation. It makes sense because local minima are less likely to have a value above μ . Let $\varphi(\cdot)$ denote the probability density function (PDF) of the standard normal distribution.

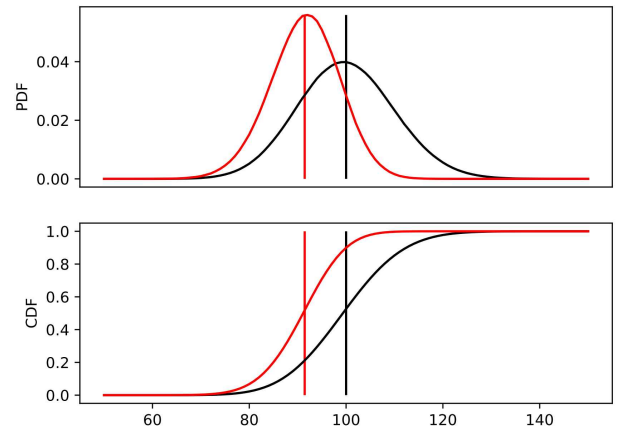


Fig. 4: Local minima's expectation bias for $\mu = 100$. Black is associated with the full signal, red is associated with its local minima. Vertical lines indicate expectations of the distributions.

Property 3: One has:

$$\begin{cases} \mathbb{E}(y_{\xi_i}) &= \mu_{\xi_i} + \sigma_{\xi_i} \frac{C_1}{C_0} \\ \mathbb{V}(y_{\xi_i}) &= \sigma_{\xi_i}^2 \left(\frac{C_2}{C_0} - \left(\frac{C_1}{C_0} \right)^2 \right) \end{cases} \quad (14)$$

where

$$C_i = \int_{-\infty}^{+\infty} u^i \varphi(u) (1 - \Phi(u))^2 du \quad (15)$$

Note that C_0 is the density of ξ for a stationary signal. Numerical integration results in the following values:

$$\begin{cases} C_0 = & 1/3 \\ C_1 \approx & -0.28209479 \\ C_2 \approx & 0.42522148 \end{cases} \quad (16)$$

The reduction of the variance of the local minima that one noticed on Fig. 4 may now be quantified:

$$\frac{V(y_{\xi_i})}{\sigma_{\xi_i}^2} = \frac{C_2}{C_0} - \left(\frac{C_1}{C_0}\right)^2 \approx 0.55946721 \quad (17)$$

Property 3 allows one to propose a bias correction:

Property 4: $\hat{\mu}_{\xi_i}$ is an unbiased estimator of μ_{ξ_i} such that:

$$\begin{cases} \hat{\mu}_{\xi_i} = & y_{\xi_i} - \sigma_{\xi_i} \frac{C_1}{C_0} \\ V(\hat{\mu}_{\xi_i}) = & V(y_{\xi_i}) \end{cases} \quad (18)$$

Proof of properties 3 and 4 is given in the appendix.

2) *Occurrence of local minima:* One have reported on the Fig. 5 the evaluation by simulation of the probability P_{min} that a point of a linear signal, with a slope γ and a gaussian noise with a standard deviation level σ , is a local minima. Note that $P_{min}(\gamma/\sigma = 0) = C_0$, and P_{min} quickly decreases.

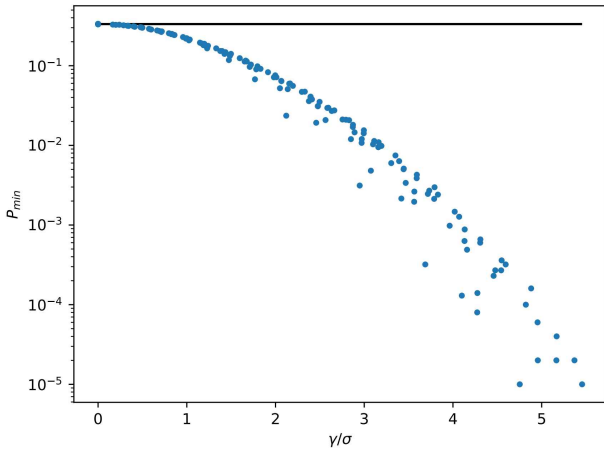


Fig. 5: Blue points represent $P_{min}(\gamma/\sigma)$ on a grid of 20 values of γ linearly spaced on $[0, 100]$ and 20 values of σ spaced evenly on a log scale on $[1, 1000]$. Black line represents C_0 .

Additionally, one can deduct from property 2 an upper bound on the probability that a local minima belongs to \mathbb{F} :

Property 5:

$$P(k \in \mathbb{F} | k \in \xi) \leq \frac{A_k}{P(k \in \xi)} \quad (19)$$

Proof of property 5 is given in the appendix. One notices that $P(k \in \xi)$ can not be too small, because in practice there is always a non negligible portion of local minima in a measurement. Moreover, Fig. 5 testifies that $\forall k \in \mathbb{F}$, A_k is dramatically low. Therefore, $P(k \in \mathbb{F} | k \in \xi)$ is majorated by a constant close to zero, which explains a remarkable phenomenon easily noticeable through data: local minima are absent from the flanks. It is thus possible to identify points in $\bar{\mathbb{F}}$ by observing ξ :

Hypothesis 2:

$$\xi \subset \bar{\mathbb{F}} \quad (20)$$

Since local minima are easily observable in a given spectrum, hypothesis 2 is a convenient criterion upon which one may build an estimator for the continuum.

III. CONTINUUM ESTIMATION

A. Intruders filtering

In the previous section, one identified points from $\bar{\mathbb{F}}$. However, this is not exactly what one was looking for (we are looking for \mathbf{c} where \mathbf{m} is omitted). Some undesirable intruders are present in ξ , as shown in Fig. 6. Indeed, it contains top points which must be removed. Moreover, local minima may accidentally appear on the flank of a significant peak. In any case, all intruders values are substantially higher than those of the points attached to the continuum. This gives us an opportunity to filter them. One assumes y_{ξ_i} is a sample from a random variable Y_i^{\min} such that:

Hypothesis 3:

$$Y_i^{\min} \sim \mathcal{N}(E(y_{\xi_i}), V(y_{\xi_i})) \quad (21)$$

Note that Hyp. 3 is actually an approximation of the true distribution of the local minima, but which simplifies the definition of the process of discontinuity detection.

Let define the null hypothesis H_0 : \ll there is no discontinuity between ξ_{i-1} and ξ_i : \gg . Let t_{break} be the $1 - \eta/2$ order quantile of $\mathcal{N}(0, 1)$ and:

$$z_i = \frac{|\Delta y_{\xi_i}|}{\sqrt{V(y_{\xi_i}) + V(y_{\xi_{i-1}})}} \quad (22)$$

By Hyp. 3, the variable z_i is a z-score for H_0 . Consequently, if $t_{\text{break}} \leq z_i$, one can reject H_0 with a confidence η .

By selecting a threshold t_{break} for this hypothesis testing, one detects discontinuities in ξ , and forms groups of continuous ξ sets. Then one observes the sign of Δy_{ξ_i} at the groups borders. This reveals groups which levels are higher than those of their direct neighbours. These are intruders groups to be filtered as shown on Fig. 6.

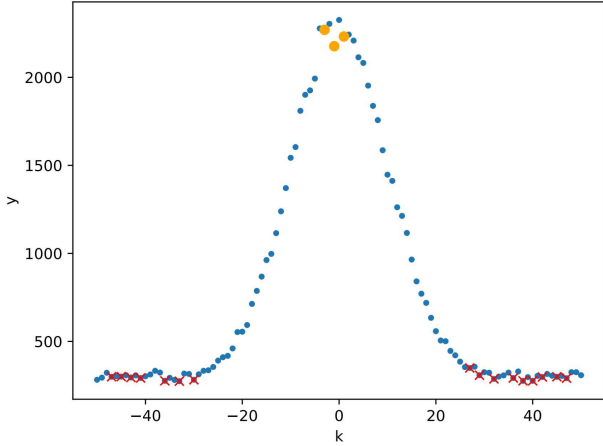


Fig. 6: Intruders filtering with $t_{\text{break}} = 1.5$. Blue points represent observations \mathbf{y} , red crosses represent remaining ξ after intruders filtering, orange points represent intruders.

B. Large peaks issue

Previous intruders filtering is able to deal with GeHP thin peaks spectra. But when facing peaks acquired by a scintillator, peaks are very large with respect to \mathbb{F} variations, and the estimator fails as shown on the top plot in Fig. 7. A simple solution is to subsample the signal before filtering the intruders as shown on the middle plot in Fig. 7. This means that from the relevant spectrum, one keep one point out of p , starting at point s . Parameter p is the subsampling step, s the subsampling offset such as $0 \leq s < p$. In this manner, the variation rate between two points is multiplied by p , whereas the noise level has not changed, which allows to fix the large peaks issue.

To limit the information loss due to subsampling, one selections subsamples of ξ successively with all possible values of s for a given p in order to produce p subsets of points of the continuum. Then subsets are merged as illustrated on the bottom plot in Fig. 7.

Actually, when facing large peaks, subsampling is a trick which allows to fall back on a thin peaks analysis issue. An optimum choice for p depends on (i) w , the actual full width at half maximum (FWHM) of the peaks and on (ii) w_{opt} , a fix ideal FWHM that one strives to retrieve. This offers a meaningful alternative parametrization for the estimator:

$$p = \max \left(1, \left\lfloor \frac{w}{w_{\text{opt}}} \right\rfloor \right) \quad (23)$$

C. Noise filtering and interpolation

In previous developments, one found points ξ in the signal where peak levels are negligible. However, the continuum has yet to be dissociated from the observation noise by a filtering operation. Furthermore, one has to fill

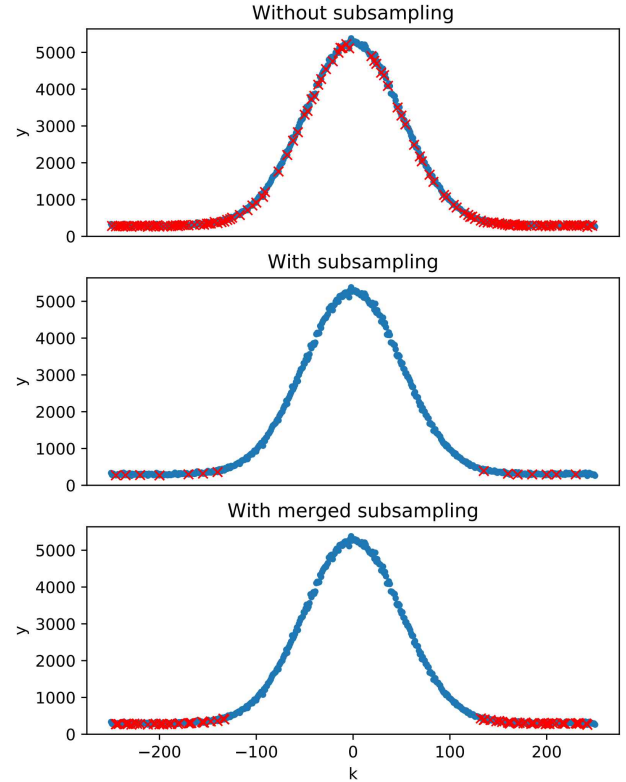


Fig. 7: Subsampling effect on outlier filtering with $t_{\text{break}} = 1.5$. Top figure uses no subsamplings, middle figure uses subsampling ($p = 5$, $s = 0$), bottom figure uses merged subsamplings ($p = 5$). Blue line represents observations \mathbf{y} , red crosses represent remaining ξ after intruders filtering.

missing values at channels which does not present local minima.

Every filter is built on a regularity prior for the clean signal that one strives to retrieve. The smoothness of the continuum suggests it can locally be described by a polynomial expression. If continuum presents some discontinuities which undermines the polynomial assumption, these are difficult to take into consideration because of our ignorance of the continuum and one merely assumes this event is rare and sets it aside.

The proposed filtering process at ξ_i then consists in the fit of a polynomial of order o_f on a odd window of w_f contiguous points of ξ centered in ξ_i . This filter is similar to a Savitzky-Golay filter [35] but with a nonuniform sampling step as points of ξ are not evenly spaced. In a second time, a linear interpolation fills the missing parts of the signal.

The selection of the appropriate window size and order achieves a trade-off between noise reduction and avoiding the introduction of bias. Indeed, the wider the window

and the lower the order, the more noise is filtered out. However, the more the noise reduction is, the less the filter will succeed to follow the continuum variations, and thus lead to a bias in the result.

In order to visualize this trade-off, let proceed to two simulations. In the first simulation, one filters the noisy observation of a constant continuum, in order to isolate the noise reduction. The variance of the noise was fixed at a level of 300. Noise reduction is then quantified by the Mean Square Error (MSE). In the second simulation, one filters a step signal without noise in order to isolate the bias. This is the worst-case scenario for the continuum variations. The step levels were fixed at 0 and 300. Filtering bias is then quantified by the MSE. The simulations results are illustrated on Fig. 8. If numeric values are specific to the simulation parameters, the graph allows to identify the dynamics of the filter.

Because of our ignorance of the continuum, there is no optimal set of parameters for the filter. Therefore, one proposes the following qualitative reasoning. Considering high continuum variations are rare events, the noise reduction is our priority selection criterion. The graph shows $o_f \in \{2, 3\}$ have the worst noise reduction score, and one rejects these. Looking at the bias score, one finally chose to set $o_f = 1$. Looking back to the noise reduction, one notes $w_f = 11$ results in $\approx 85\%$ of noise reduction and does not improve that much for greater values. Therefore, one chose to set $w_f = 11$.

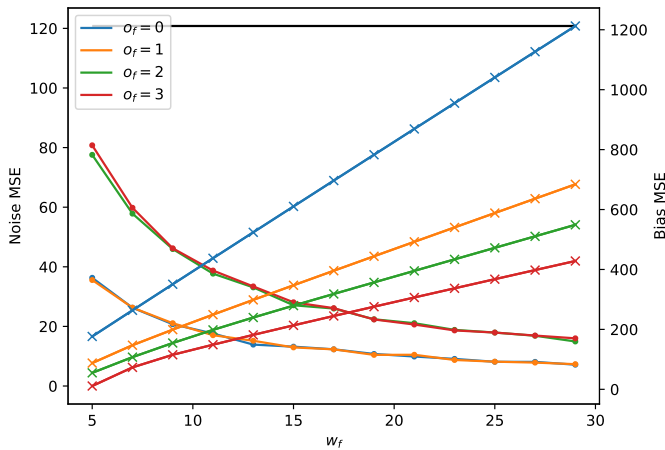


Fig. 8: Evolution of the MSE with the window size for several orders. Points are resulting from the noise reduction simulation. Black line represents the observation noise level. Crosses are associated to the filtering bias simulation. Colors are associated to a given value for o_f according to the legend. Unobservable blue points are hidden behind orange points. Unobservable green points are hidden behind red points.

D. Full continuum estimation procedure

For a given spectrum, the full continuum estimation procedure is the following: 1) subsampling the signal as in part III-B; 2) observing local minima defined in (13); 3) filtering intruders as in part III-A; 4) correcting the local minima bias by property 4; 5) merging remaining points from each subsamples; 6) filtering noise and interpolating to extend the signal to all channels as in part III-C. Then the BR consists in removing the estimated continuum to the signal in order to isolate the peak mixture covered by the observation noise.

The procedure depends on w which allows to scale the effects of the process (23), and on the parameters t_{break} , w_{opt} , w_f and o_f . An illustration of the resulting full estimation is reported in Fig. 9. One notes that the peak is essentially extracted, even if slightly underestimated. A portion of the peak basis is indeed assigned to the continuum which biases the estimation of the area. This is inevitably caused by the bordering areas where it is difficult to assign a point to \mathbb{F} or $\overline{\mathbb{F}}$.

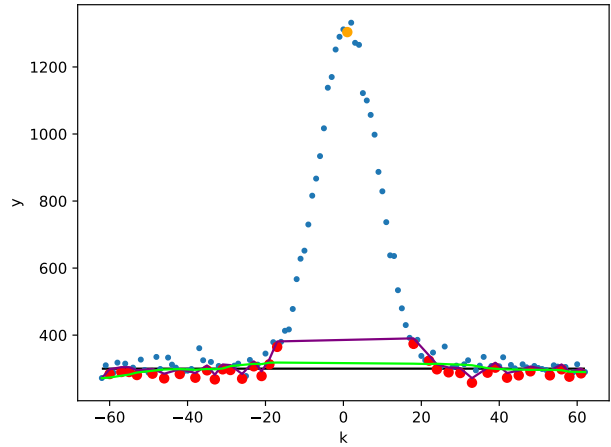


Fig. 9: Continuum estimation. Black line represents \mathbf{c} . Blue points represent observations \mathbf{y} . Red points represent remaining ξ after intruders filtering. Orange points represent intruders. Purple line is the continuum estimation without noise filtering, with $w = 18$, $t_{break} = 1.3$ and $w_{opt} = 15$. Green line is the full continuum estimation with $w_f = 11$ and $o_f = 1$.

Fig. 9 also reports the continuum estimation without the use of the filter, from which it can be seen that the bias of the filter attenuates the bias of the estimator. Fig. 10, generated by Monte Carlo simulations, details this effect by showing the expected continuum estimate as a function of the filtering window. It also shows that the continuum estimate slightly extends beyond the base of the peak.

E. Selection of parameters

The mean width of the peaks w is constant for a given measurement device, but still needs to be (roughly)

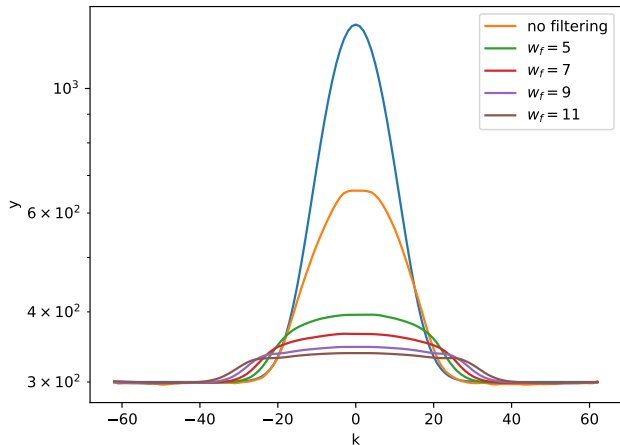


Fig. 10: Filtering attenuation of the continuum bias. Blue line represents μ , the signal without noise. Other lines are the expected estimation of the continuum, varying w_f , with $w = 18$, $t_{\text{break}} = 1.3$ and $w_{\text{opt}} = 15$.

specified in order to adapt the method to the spectrometer. Filters parameters were fixed in III-C to $w_f = 11$ and $o_f = 1$, and this choice is confirmed by Fig. 10.

Parameters t_{break} and w_{opt} allow to define the balance between peaks and continuum, but are still unspecified. As the area of the peaks in the spectrum are the measurand of the spectrometry gamma analysis, the bias on the estimated area is a relevant metric of the goodness of the continuum estimation.

A set of grid explorations were performed on Monte Carlo simulation for several configurations for the estimator and for the spectrum. Each simulation is repeated 500 times. The simulated signal is a Gaussian peak characterized by a FWHM w and a height h added to a constant continuum c covered by a Poisson noise (the same configuration as the one of the signal of Fig. 9). The baseline removal process is then applied to the signal, but without noise filtering in order to isolate the influence of t_{break} and w_{opt} . The area of the peak is estimated from the difference of the observation and of the continuum estimate. The expected bias on the estimated area was reported on Fig. 11.

It may be seen on Fig. 11a that without subsampling, only well resolved peaks (with small w) are properly managed by the method. As a consequence, the application range of the estimator of Tervo is roughly limited to $w < 15$. The confrontation of Fig. 11a and Fig. 11b shows the contribution of the subsampling, which extend the method to any peak width. Apparent lines of discontinuity in Fig. 11b are associated with a change in the subsampling step p .

Fig. 11d shows that t_{break} is little sensitive to the choice for w_{opt} . As a consequence, t_{break} and w_{opt} can be chosen

independently.

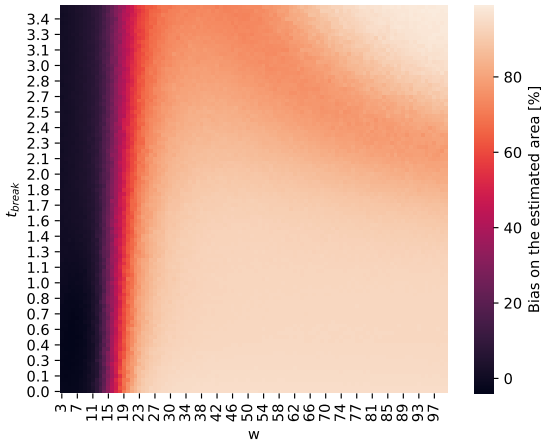
Fig. 11a and 11c show that t_{break} is not sensitive to the width of the peak, but to the noise level. Indeed, faced to significant peaks, i.e. clearly distinguishable from the noise, outlier filtering does not impact that much the average estimator performance, because it is designed to deal with rare events. When a local minima appears on the top of a peak, a too high value of t_{break} will prevent to detect the outliers. However, the acceptable limit value is high, because variations between points of the continuum and points of the top of the peak are huge. Conversely, a too small value of t_{break} will exclude a lot of local minima from the pure continuum. This loss will be amplified by the continuum variation. As a consequence, one cautiously chose to set $t_{\text{break}} = 3$.

By observing Fig. 11, one is tempted to chose the smallest admissible value for w_{opt} . However, the simulations does not consider variations in the continuum and the application to real spectra will not be satisfactory because large parts of the pure continuum will be excluded from the estimate. In the absence of any characterization of the continuum variations, it is mandatory to proceed to an extensive empirical campaign in order to select w_{opt} , for which the goodness of the estimate relies on the visual validation of an expert. The authors figure out that $w_{\text{opt}} = 15$ is an empirical robust choice.

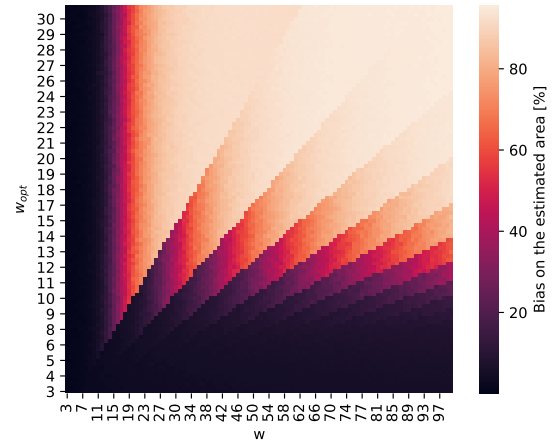
IV. REAL SPECTRA APPLICATION

Fig. 1 and 12 present real spectra continuum estimations in order to permit a comparison between the method of Tervo [27] and the proposed method. One notices that the estimator of Tervo appears to be a particular case of the new estimator without filtering, with a different interpolation method, and with $t_{\text{break}} = +\infty$ and $w_{\text{opt}} = +\infty$. Undoubtedly, the new estimator shows enhanced performances and qualitatively meets our expectations in both applications since almost all significant peaks that one may visually identify are extracted. To the knowledge of the authors, no relevant quantitative performance metrics exists for such estimators because continuum are by essence unknown quantities. All reference metrics are resulting from a visual quality assessment, which does not add anything to the examination of the proposed figures.

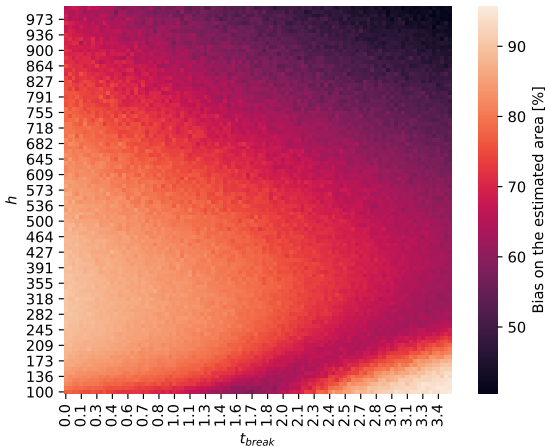
Fig. 12a shows the efficiency of the new procedure. The noise reduction is satisfying. The areas [300, 400] and [4600, 4800] show it conveniently deals with multiplets. The area [500, 540] presents the largest continuum variation of the spectrum, and the new method is slightly biased. It is attributed to the noise filter, because Tervo's estimation is not biased. Tervo's estimator gives large bias in areas [4300, 4400], [4600, 4800] and [6200, 6600], which does not happen to the new procedure. Little peaks [2100, 2250], [3400, 3500], [3900, 4000] and [5300, 5500] are correctly separated from the continuum by the new procedure, which is not the case with Tervo's estimation.



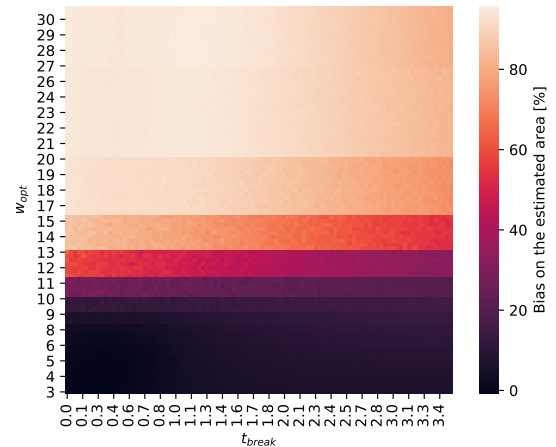
(a) Omission of subsampling ($h = 1000, p = 1$).



(b) Contribution of the subsampling ($h = 1000, t_{\text{break}} = 1.5$).



(c) Influence of the noise level on t_{break} ($w = 18, p = 1$).



(d) Influence of t_{break} ($h = 1000, w = 80$).

Fig. 11: The expected bias on the estimated area for several configuration of the continuum estimator. The continuum level is fixed to $c = 300$. Filtering parameters are fixed to $w_f = 11$ and $o_f = 1$. The shade of colours indicates the relative values of the bias.

Fig. 12b shows the adaptability and the robustness of the new procedure, where Tervo's method fails. The proximity of peaks and continuum variations in the area [600, 900] suggests the estimate can be unstable in this area. However, the estimate seems to be satisfying, which shows the robustness of the continuum estimate to continuum variations. The new estimator fails in area [300, 400] because of the conjugated effect of the noise filtering and of the continuum discontinuity. It is not convincingly dealing with the multiplet in the area [3400, 3800] because the peaks ratio of height to width is too low. Elsewhere, peaks were conveniently removed from the continuum estimate.

V. CONCLUSION

This paper deduces the properties of local minima under an original aspect, i.e. counter variations, and proposes a totally new estimation procedure, for which the key parts are intruders filtering and subsampling. The present work stands as an improvement of the method of Tervo et al. [27], which is limited by the FWHM of the measurement spectra, does not handle the apparition of local minima on top of peaks, does not filter the noise and relies on over-sophisticated interpolation process.

A full optimization procedure of the parameters, and a study of the robustness of the method would be appreciated. However, in the absence of a more accurate description for the continuum, this appears to be unreachable. Nevertheless, the proposed empirical adjustment should fit

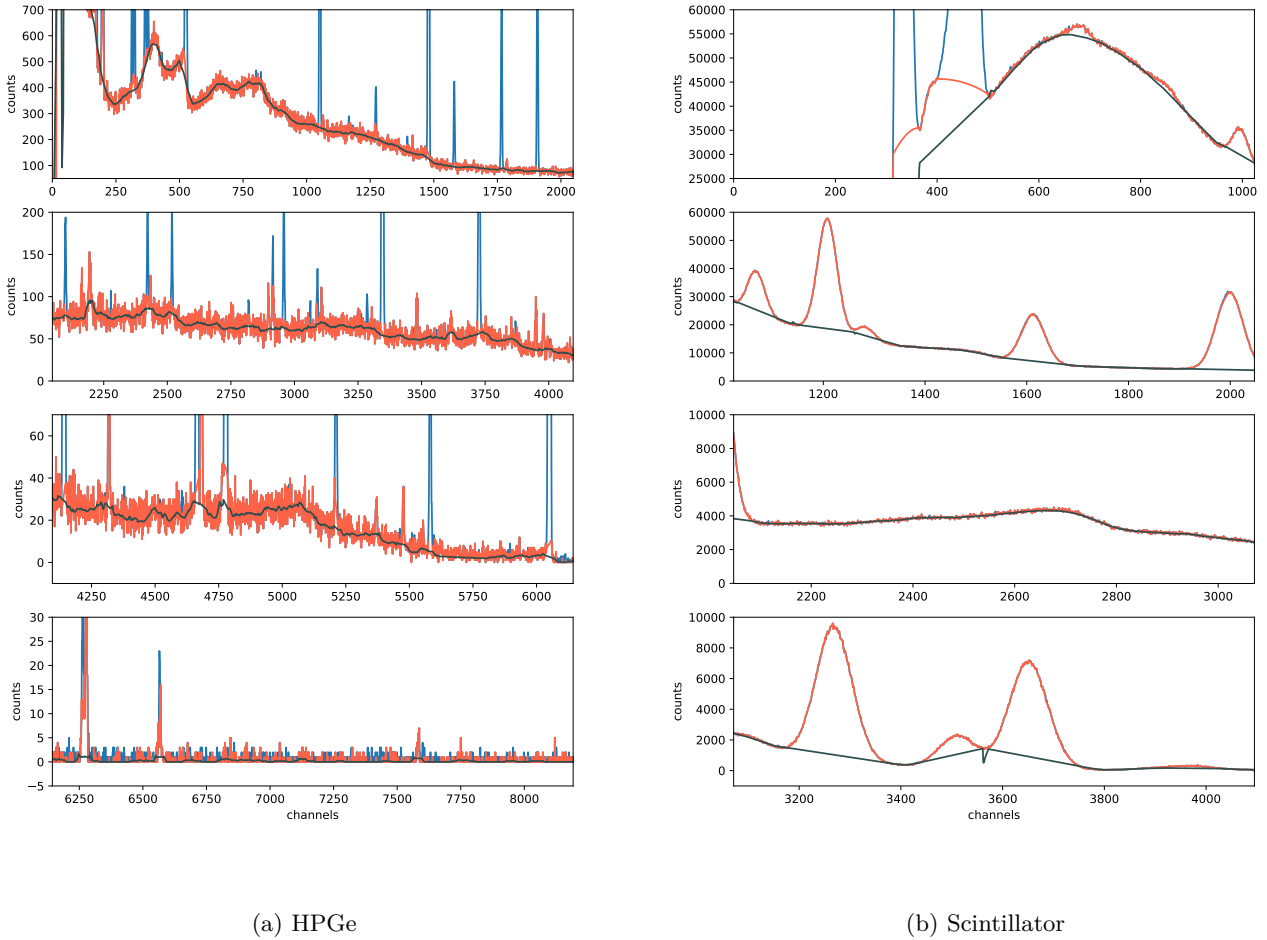


Fig. 12: Zoom on the continuum estimation of spectra of Fig. 1. The plot uses a linear scale. Blue lines represent the observation. Orange lines represent the reference estimates of Tervo's method. Black lines represent the new method results, applied with parameters $t_{\text{break}} = 3$, $w_{\text{opt}} = 15$, $w_f = 11$, $o_f = 1$ and $w = 6$ for HPGc, $w = 80$ for scintillator.

for a general purpose, and the authors are of the opinion that little performances improvement is to be expected in this direction. Naturally, this method presents some limits when continuum variations are close to peaks variations.

As a conclusion, this method allows a quick, robust, adaptive and automated baseline removal for gamma spectrum. It can be used as a preprocessing operation to the peak mixture analysis.

APPENDIX

Proof of properties 3 and 4: Let consider a stationary signal of three channels simulated with $X_1, X_2, X_3 \sim \mathcal{N}(\mu, \sigma^2)$. Let $f_{X_i}(\cdot)$ denote their PDF and $g(x) = \frac{x - \mu}{\sigma}$. Consequently:

$$\begin{cases} f_X(x) = g'(x)\varphi(g(x)) \\ P(X_i \leq x) = \Phi(g(x)) \end{cases} \quad (24)$$

One is looking for f , the conditional PDF of X_2 when it turned out to be a local minima:

$$f(x) = f_{X_2|X_2 < X_1, X_2 < X_3}(x) \quad (25)$$

$$\propto f_{X_2}(x)P(x < X_1)P(x < X_3) \quad (26)$$

$$\propto f_{X_2}(x)(1 - P(X_1 < x))^2 \quad (27)$$

$$\propto g'(x)\varphi(g(x))(1 - \Phi(g(x)))^2 \quad (28)$$

Let assess the normalization constant:

$$\int_{-\infty}^{+\infty} g'(t)\varphi(g(t))(1 - \Phi(g(t)))^2 dt = \int_{-\infty}^{+\infty} \varphi(u)(1 - \Phi(u))^2 du \quad (29)$$

$$= C_0 \quad (30)$$

Thus $f(x) = \frac{1}{C_0}g'(x)\varphi(g(x))(1 - \Phi(g(x)))^2$. Let Z a random variable with f as PDF. Involving variable

mutation:

$$\mathbb{E}(Z) = \int_{-\infty}^{+\infty} tf(t)dt = \int_{-\infty}^{+\infty} (\sigma g(t) + \mu)f(t)dt = \sigma \frac{C_1}{C_0} + \mu \quad (31)$$

$$\Leftrightarrow \mathbb{E}\left(Z - \sigma \frac{C_1}{C_0}\right) = \mu \quad (32)$$

which endorses the proposed estimator. Then:

$$\mathbb{E}(Z)^2 = \left(\sigma \frac{C_1}{C_0} + \mu\right)^2 \quad (33)$$

$$= \left(\sigma \frac{C_1}{C_0}\right)^2 + 2\sigma\mu \frac{C_1}{C_0} + \mu^2 \quad (34)$$

Moreover:

$$\mathbb{E}(Z^2) = \int_{-\infty}^{+\infty} t^2 f(t)dt = \int_{-\infty}^{+\infty} (\sigma g(t) + \mu)^2 f(t)dt \quad (35)$$

$$= \int_{-\infty}^{+\infty} (\sigma^2 g(t)^2 + 2\sigma\mu g(t) + \mu^2)f(t)dt \quad (36)$$

$$= \sigma^2 \frac{C_2}{C_0} + 2\sigma\mu \frac{C_1}{C_0} + \mu^2 \quad (37)$$

Let derive the variance of this estimator:

$$\mathbb{V}\left(Z - \sigma \frac{C_1}{C_0}\right) = \mathbb{V}(Z) = \mathbb{E}(Z^2) - \mathbb{E}(Z)^2 \quad (38)$$

$$= \sigma^2 \left(\frac{C_2}{C_0} - \left(\frac{C_1}{C_0}\right)^2\right) \quad (39)$$

Proof of property 5: One has

$$P(k \in \mathbb{F}) = P(k \in \mathbb{F}^+) + P(k \in \mathbb{F}^-) \quad (40)$$

Furthermore:

$$P(k \in \xi | k \in \mathbb{F}^+) = P(\Delta Y_k < 0, \Delta Y_{k+1} > 0 | \alpha \leq \Delta m_k) \quad (41)$$

$$\leq P(\Delta Y_k < 0 | \alpha \leq \Delta m_k) = F_k \leq A_k \quad (42)$$

In the same way, one finds $P(k \in \xi | k \in \mathbb{F}^-) \leq A_k$. Therefore:

$$P(k \in \xi | k \in \mathbb{F}) = P(k \in \xi | k \in \mathbb{F}^+) \frac{P(k \in \mathbb{F}^+)}{P(k \in \mathbb{F})} \quad (43)$$

$$+ P(k \in \xi | k \in \mathbb{F}^-) \frac{P(k \in \mathbb{F}^-)}{P(k \in \mathbb{F})} \quad (44)$$

$$\leq \frac{A_k}{P(k \in \mathbb{F})} (P(k \in \mathbb{F}^+) + P(k \in \mathbb{F}^-)) \quad (45)$$

$$= A_k \quad (46)$$

Finally:

$$P(k \in \mathbb{F} | k \in \xi) = P(k \in \xi | k \in \mathbb{F}) \frac{P(k \in \mathbb{F})}{P(k \in \xi)} \quad (47)$$

$$\leq \frac{A_k}{P(k \in \xi)} \quad (48)$$

■

REFERENCES

- [1] Bertrand Pérot, Fanny Jallu, Christian Passard, Olivier Gueton, Pierre-Guy Alline, Laurent Loubet, Nicolas Estre, Eric Simon, Cédric Carasco, Christophe Roue, et al. The characterization of radioactive waste: a critical review of techniques implemented or under development at cea, france. *EPJ Nuclear Sciences & Technologies*, 4:3, 2018.
- [2] Gordon Gilmore. *Practical Gamma-Ray Spectrometry*. John Wiley & Sons, 2 edition, 2011.
- [3] Canberra. *Genie2000 v3.1. Customization tools manual*, 2006.
- [4] László Szentmiklósi. Fitting special peak shapes of prompt gamma spectra. *Journal of Radioanalytical and Nuclear Chemistry*, 315(3):663–670, 2018.
- [5] Georg Schulze, Andrew Jirasek, ML Marcia, Arnel Lim, Robin FB Turner, and Michael W Blades. Investigation of selected baseline removal techniques as candidates for automated implementation. *Applied spectroscopy*, 59(5):545–574, 2005.
- [6] P Quittner. Peak area determination for ge (li) detector data. *Nuclear Instruments and Methods*, 76(1):115–124, 1969.
- [7] L Varnell and J Trischuk. A peak-fitting and calibration program for ge (li) detectors. *Nuclear Instruments and Methods*, 76(1):109–114, 1969.
- [8] Jorma T Routti and Stanley G Prussin. Photopeak method for the computer analysis of gamma-ray spectra from semiconductor detectors. *Nuclear instruments and methods*, 72(2):125–142, 1969.
- [9] Karsten Normann Thomsen, Jette Nørgaard Pedersen, and Niels Pind. Procedure for background estimation in energy-dispersive x-ray fluorescence spectra. *Analytica chimica acta*, 184:133–142, 1986.
- [10] Y Kawarasaki. A simple method for generation of background-free gamma-ray spectra. *Nuclear Instruments and Methods*, 133(2):335–340, 1976.
- [11] HR Ralston and George E Wilcox. A computer method of peak area determinations from ge–li gamma spectra. Technical report, California Univ., Livermore. Lawrence Radiation Lab., 1968.
- [12] LV East, RL Phillips, and AR Strong. A fresh approach to nai scintillation detector spectrum analysis. *Nuclear Instruments and Methods in Physics Research*, 193(1-2):147–155, 1982.
- [13] SA Gerasimov. *Recursive filtering of gamma ray spectra*, volume 72. Elsevier, 1992.
- [14] Zhi-Min Zhang, Shan Chen, and Yi-Zeng Liang. Baseline correction using adaptive iteratively reweighted penalized least squares. *Analyst*, 135(5):1138–1146, 2010.
- [15] Georg Winter. Continuum estimation and peak analysis for in-beam gamma ray spectra. *Nuclear Instruments and Methods in Physics Research Section A: Accelerators, Spectrometers, Detectors and Associated Equipment*, 258(1):119–126, 1987.
- [16] W Von der Linden, V Dose, and R Fischer. How to separate the signal from the background. In *MAXENT96-Proceedings of the Maximum Entropy Conference*, page 146. Citeseer, 1996.
- [17] Andreas F Ruckstuhl, Matthew P Jacobson, Robert W Field, and James A Dodd. Baseline subtraction using robust local regression estimation. *Journal of Quantitative Spectroscopy and Radiative Transfer*, 68(2):179–193, 2001.
- [18] Roland Fischer, KM Hanson, V Dose, and W von Der Linden. Background estimation in experimental spectra. *Physical Review E*, 61(2):1152, 2000.
- [19] Vincent Mazet, Cédric Carteret, David Brie, Jérôme Idier, and Bernard Humbert. Background removal from spectra by designing and minimising a non-quadratic cost function. *Chemometrics and intelligent laboratory systems*, 76(2):121–133, 2005.

- [20] Nikolaos Kourkoumelis, Alexandros Polymeros, and Margaret Tzaphlidou. Background estimation of biomedical raman spectra using a geometric approach. *Spectroscopy: An International Journal*, 27, 2012.
- [21] Zhong Li, De-Jian Zhan, Jia-Jun Wang, Jing Huang, Qing-Song Xu, Zhi-Min Zhang, Yi-Bao Zheng, Yi-Zeng Liang, and Hong Wang. Morphological weighted penalized least squares for background correction. *Analyst*, 138(16):4483–4492, 2013.
- [22] Xiaoran Ning, Ivan W Selesnick, and Laurent Duval. Chromatogram baseline estimation and denoising using sparsity (beads). *Chemometrics and Intelligent Laboratory Systems*, 139:156–167, 2014.
- [23] Kyle J Bilton, TH Joshi, MS Bandstra, JC Curtis, BJ Quiter, RJ Cooper, and K Vetter. Non-negative matrix factorization of gamma-ray spectra for background modeling, detection, and source identification. *IEEE Transactions on Nuclear Science*, 66(5):827–837, 2019.
- [24] T Inouye, T Harper, and NC Rasmussen. Application of fourier transforms to the analysis of spectral data. *Nuclear Instruments and Methods*, 67(1):125–132, 1969.
- [25] W Westmeier. Background subtraction in ge (li) gamma-ray spectra. *Nuclear Instruments and Methods*, 180(1):205–210, 1981.
- [26] TJ Kennett, WV Prestwich, and RJ Tervo. Automated analysis for high energy gamma ray spectra. *Nuclear Instruments and Methods in Physics Research*, 190(2):313–323, 1981.
- [27] RJ Tervo, TJ Kennett, and WV Prestwich. An automated background estimation procedure for gamma ray spectra. *Nuclear Instruments and Methods in Physics Research*, 216(1-2):205–218, 1983.
- [28] Miroslav Morháč. An algorithm for determination of peak regions and baseline elimination in spectroscopic data. *Nuclear Instruments and Methods in Physics Research Section A: Accelerators, Spectrometers, Detectors and Associated Equipment*, 600(2):478–487, 2009.
- [29] Miltiadis Alamaniotis, John Mattingly, and Lefteri H Tsoukalas. Kernel-based machine learning for background estimation of nai low-count gamma-ray spectra. *IEEE Transactions on Nuclear Science*, 60(3):2209–2221, 2013.
- [30] MA Mariscotti. *A method for automatic identification of peaks in the presence of background and its application to spectrum analysis*, volume 50. Elsevier, 1967.
- [31] ISO-19017:2015(en). Guidance for gamma spectrometry measurement of radioactive waste, 2015.
- [32] ASTM Standard et al. Standard test methods for detector calibration and analysis of radionuclides. 2011.
- [33] This Kélian, Laurent Le Brusquet, Frigerio Adrien, Colas Sébastien, and Bondon Pascal. Contribution to continuum estimation in gamma spectrum by observation of local minima. In *2020 24th International Conference on System Theory, Control and Computing (ICSTCC)*, pages 937–942. IEEE, 2020.
- [34] Gilbert Saporta. *Probabilités, analyse des données et statistique*. Editions Technip, 2006.
- [35] Abraham Savitzky and Marcel JE Golay. Smoothing and differentiation of data by simplified least squares procedures. *Analytical chemistry*, 36(8):1627–1639, 1964.